ACS APPLIED NANO MATERIALS

www.acsanm.org Article

First-Principles Calculations Predict Tunable Large Magnetic Anisotropy Due to Spin-Polarized Quantum-Well Resonances in Nanometer-Thick $SrRuO_3$ Films: Implications for Spintronic Devices

Angus Huang, Horng-Tay Jeng,* and Ching-Hao Chang*

Cite This: *ACS Appl. Nano Mater.* 2021, 4, 5932−5939 Read Online

ACCESS | Metrics & More | Article Recommendations | Supporting Information

ABSTRACT: We demonstrate that the magnetic anisotropy in $SrRuO_3$ (SRO) ultrathin films can be well controlled by thickness or electrical modulations: The easy axis (preferred magnetization direction) of a SRO ultrathin film can be switched between out-of-plane and in-plane magnetization either by altering the film thickness or by tuning the doping level through applying a gate voltage or chemical doping. Such a capability to manipulate the magnetocrystalline anisotropy energy (MCAE) is given by the spin−orbit coupling (SOC)-induced energy splitting in the spin-polarized quantum well states (QWSs) near the Fermi level. These QWSs are susceptible to the intrinsic spin−orbit interaction and thus drive a large energy discrepancy when an SRO ultrathin film rotates its magnetization direction. As a result of the MCAE nature, a SRO film has a magnetic anisotropy approximately an order of magnitude larger than those in 3d-ferromagnet ultrathin films and its easy-axis direction depends on the film thickness, gate voltage, and substrate. This tunable large magnetic anisotropy in SRO ultrathin films provides an excellent route toward advanced spintronic devices such as storage and memory devices.

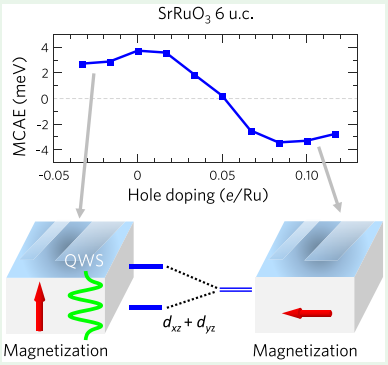

KEYWORDS: *strontium ruthenate, quantum well states, spintronics, magnetocrystalline anisotropy, spin−orbit coupling*

INTRODUCTION

Nanoscaled magnetic-tunneling-junction devices, including solid-state drive (SSD)[1] and magnetoresistive random access memory (MRAM) devices,[2−4] are extremely important for their high potential for extensive applications. A key character of these devices is the MCAE, which measures the energy difference between magnetic states with different magnetization orientations. To gain the ability to control the easy axis in magnetic devices through selecting materials with suitable properties, tailoring the device geometry, and/or applying a gate voltage, a microscopic understanding of the MCAE origin is thus indispensable.

Ultrathin films of strontium ruthenate $SrRuO_3$ (SRO, known as SRO113) have attracted great attention for they are predicted to have unique spintronics properties, such as the quantum anomalous Hall effect[5] and two-dimensional half-metallic electron gas.[6] Novel magnetic properties, such as spin-transfer torque[7] and spin current,[8] can be induced and tailored in magnetic complex oxides by external system factors. In addition, the switching of ferroelectric resistance was observed recently in the SRO/ferroelectric heterostructure.[9,10] The dramatic modulations of the SRO magnetic properties are found to be driven by the intrinsic nonstoichiometric properties of the SRO system.[11,12] In this respect, the MCAE effect in a SRO thin film is an important research direction that has been investigated in many experimental works in the past half-century.[13−17] The magnetic anisotropy is observed to be much stronger than those in 3d ferromagnet films (such as Fe and Co films)[18,19] and can be altered dramatically by selecting a substrate that introduces a large interfacial strain to change the lattice constant and rotate the Ru−O−Ru bond angle.[20,21] The easy magnetic axis in SRO films, however, is somewhat confusing for its direction can be either in plane or out of plane in different pioneer studies[13,14,21] This indicates that the easy axis significantly depends on the conditions in the SRO sample, including its film thickness,[22] detailed lattice structure,[13,14,21] and substrate material.[23]

The microscopic origin of the MCAE and easy axis in 3d ferromagnet films have been investigated extensively and exhaustively in studies based on experimental measurements and theoretical models. The spin-polarized quantum well states (QWSs) are confirmed to significantly contribute to the MCAE.[24−27] Different spins and groups of the QWSs,[24,28,29] surface states,[30,31] and intrinsic and interfacial spin−orbital interactions[32−36] are found to cooperate to induce the MCAE.

Received: March 25, 2021
Accepted: May 7, 2021
Published: May 20, 2021

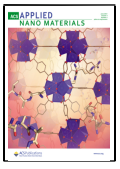

Moreover, the positive or negative sign of the QWSs-induced MCAE directly decides whether the direction of the easy axis is out of plane and in plane, respectively.[37,38] Crucially, the spin-polarized d_{xz} and d_{yz} QWSs have been observed in SRO(001) ultrathin films recently.[39] Investigation of the MCAE due to the QWSs opens routes to study the nature of the magnetocrystalline anisotropy and also how to tune it.

A quantum well state is electronic state of an ultrathin film confined by the boundaries, such as the cap layer and substrate. When the film thickness varies, the QWS may pass through the Fermi level, inducing huge changes in the DOS near the Fermi level. This dramatic DOS change thus dominates the material properties, such as thermal stability,[40] effective mass,[41,42] work functions,[43] surface energy,[44−46] interlayer exchange coupling,[47] and superconductivity critical temperature,[48,49] as presented in previous experiments and theories. Yet, a clear picture and deep understanding for the relation between quantum confinement (which leads to the QWSs formation), spin−orbit coupling, and magnetocrystalline anisotropy have not been shown to date.

In this article, we study the SRO(001) ultrathin film using density functional theory. We start with the $SrRuO_3$ simple perovskite structure called "bulk SRO". We then stack the bulk SRO unit cell to form symmetric SRO ultrathin films with thickness varying from 3 to 15 unit cells, which correspond to a stoichiometry of $Sr_{n+1}Ru_nO_{3n+1}$ with n = 3−15. As revealed in experiments,[6] SRO films with such thickness show metallic ferromagnetism. From DFT simulation, we show that the magnetic easy axis of a SRO ultrathin film switches between in plane (100 direction, $\mathbf{M}\perp\mathbf{z}$, as shown in Figure 1a) and out of plane (001 direction, $\mathbf{M}\|\mathbf{z}$) due to the d_{xz} and d_{yz} QWSs with spin−orbital coupling. We further demonstrate that both the sign and the magnitude of the MCAE in a SRO(001) ultrathin film can be tuned by shifting the energy of the QWSs by geometrically adjusting the film thickness or electrically applying a gate voltage. This flexibility of controlling the magnetocrystalline anisotropy of a SRO ultrathin film indicates that this film has high potential for advanced spintronic devices.

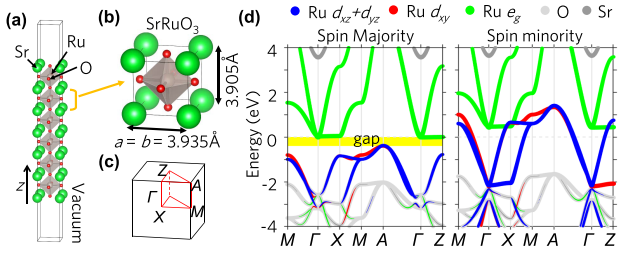

Figure 1. (a) Lattice structure of a 6-u.c SRO ultrathin film. (b) One unit cell in the SRO ultrathin film. (c) First Brillouin zone and high-symmetry points of bulk SRO. (d) Spin- and orbital-resolved band structures of bulk SRO. Left and right panels are the majority and minority spin channels, respectively. Size and color of the dots indicate the components from different orbitals and ions. Moreover, yellow region presents the band gap of spin majority.

ELECTRONIC STRUCTURES OF $SRRUO_3$ FILM

To understand the nature of the QWSs in the SRO ultrathin film (Figure 1a), we studied the experimental SRO films composed of a tetragonal Bravais lattice[50−52] with lattice constants a = 3.935 Å and c = 3.905 Å[23,52] in the SRO perovskite unit cell (u.c.) (Figure 1b). Experimentally, the tetragonal SRO thin film has been synthesized using suitable substrates.[23] The experimental lattice constant of 3.93 Å of the SRO tetragonal phase is adopted in this work. In this structure, each Ru ion is surrounded by six oxygen ions forming an RuO_6 octahedron. The octahedral crystal field splits the Ru 4d states into the off-axial t_{2g} and axial e_g orbitals. The Jahn−Teller distortion and rotation of the RuO_6 octahedron may be important in bulk cases of SRO. However, as reported in previous studies, the lattice distortion can be suppressed by suitably adopted substrates[52,53] and is therefore ignored in this work for simplicity. It has been demonstrated that the on-site Coulomb repulsion U is important for obtaining the correct half-metallic ground state;[54] therefore, we only present the LDA+U results here. The majority and minority bulk band structures of SRO along the high- symmetry lines of the first Brillouin zone (Figure 1c) without SOC are shown in Figure 1d. The size and color of the circles indicate the magnitude of the atomic orbital contributions. As shown, there exists an energy gap at the Fermi level between the Ru t_{2g} and the e_g bands in the majority spin channel, while the Fermi level lies in the minority Ru t_{2g} bands, providing spin-down conduction carriers. These results show the half-metallic nature of SRO, consistent with previous theoretical studies, including LDA +U[54] and GW approximations,[55] as well as with experimentally measured high-spin polarizations.[56−58]

For a SRO ultrathin film with the confinement along the z direction, both d_{xz} and d_{yz} electronic states in the minority t_{2g} bands form QWSs owing to the boundary condition, while the d_{xy} state does not form QWS as it lies in the xy plane, as observed in recent experimental measurements.[39] In the following, we will demonstrate that these thickness-dependent d_{xz} and d_{yz} QWSs can have a significant effect on the magnetocrystalline anisotropy of SRO ultrathin films, providing an excellent platform for manipulating the MCAE energies through QWSs by controlling the thickness, strain, doping, and/or gating voltage.

We note that the MCAE behavior in SRO ultrathin films studied in this work is unique in comparison with other ferromagnetic thin films such as iron and cobalt studied previously.[24,25,28,29] The former exhibits single-spin and single-class QWSs near the Fermi level, which leads to a simple relation between the MCAE and the QWSs. The latter, however, show rich classes of QWSs in a wide range of Brillouin zone and thus has a complex relation between the MCAE and the QWSs.

QUANTUM WELL STATE AND SPIN−ORBIT COUPLING IN $SRRUO_3$

Figure 2 shows the band structures of SRO ultrathin films with thicknesses of 6 and 9 unit cells (u.c.) (Figure 1b) with/without SOC. In the absence of SOC, the d_{xy} bands (red curves in Figure 2a and 2e) are similar to those in the bulk phase (blue curves in Figure 1d) while the d_{xz} and d_{yz} bands show a discrete energy level behavior owing to the QWS nature (blue curves in Figure 2a and 2e). The d_{xz} and d_{yz} QWSs keep 2-fold degeneracy at the $\bar{\Gamma}$ point and then slightly split away from the Brillouin zone center, giving rise to somewhat flat bands around the zone center. Both the energy positions and the number of QWSs change with the confinement condition given by the film thickness. In the vicinity of the Fermi level, for instance, the QWSs of the 6-u.c. SRO film (Figure 2a) locate at the Fermi level, while in the 9-

https://doi.org/10.1021/acsanm.1c00775
ACS Appl. Nano Mater. 2021, 4, 5932−5939

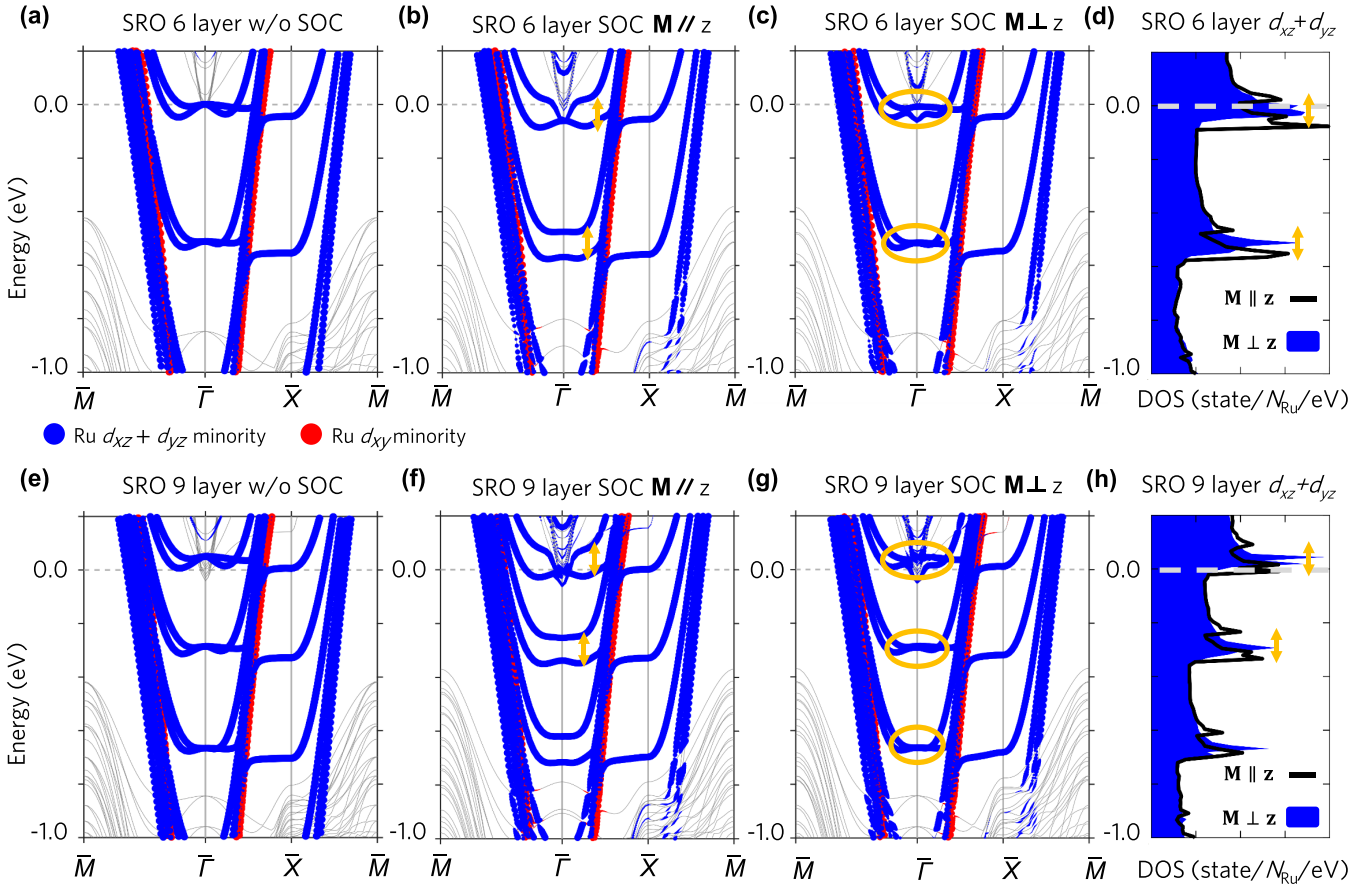

Figure 2. Minority spin band structures and density of states of 6-u.c. and 9-u.c. SRO ultrathin films. Blue (red) circles indicate the Ru d_{xz} and d_{yz} (d_{xy}) orbital components. (a and e) Minority spin band structures in the absence of SOC. (b and f) Band structures of **M**∥**z** phase with SOC. Orange arrows indicate the SOC-induced energy splits. (c and g) Band structures of **M**⊥**z** phase with SOC. Orange circles indicate negligible SOC-induced energy splits. (d and h) DOS of **M**∥**z** and **M**⊥**z** phases.

u.c. SRO film case, they shift to higher energy above the Fermi level (Figure 2e). Note that these bands around the Fermi level belong to different quantum numbers of the QWSs in the 6-u.c. and 9-u.c. cases.

The SOC given by the perturbative approach has the form $H_{SO} = \lambda_{SO}\mathbf{L} \times \mathbf{S} = \lambda_{SO}(L_+\sigma_- + L_-\sigma_+ + L_z\sigma_z)/2$, where σ (L) is the Pauli matrix (orbital angular momentum) and λ_{SO} is the material-dependent SOC parameter indicating the spin−orbit coupling strength. For orbitals $d_{xz} = (|-1\rangle - |1\rangle)/2$ and $d_{yz} = (|-1\rangle + |1\rangle)/2$ with ±1 being the magnetic quantum numbers, all of the matrix elements of operator $L_\pm$ are zero in the $\{d_{xz},d_{yz}\}$ basis. Hence, the d_{xz} and d_{yz} QWSs are only influenced by the z component of H_{SO}

$$H_{SO}^{eff} = H_{SO}^{(z)} = \lambda_{SO}L_z\sigma_z/2 \quad (1)$$

The minority spin band structures (SOC included) of the 6-u.c. and 9-u.c. SRO films with different magnetizations, i.e., parallel and perpendicular to the SRO film normal, are shown in Figure 2b and 2c and Figure 2f and 2g, respectively. Since the above equation is similar to the Hamiltonian of the Zeeman effect, the degeneracy of the magnetic quantum numbers $m_l = \pm 1$ at the $\bar{\Gamma}$ point is equivalent to the Kramers degeneracy. When the magnetization is along the z direction (**M**∥**z** or 001 direction), eq 1 acts as an effective Zeeman term to split states $|-1\rangle$ and $|1\rangle$. This leads to a large energy split of ≃0.1 eV around the $\bar{\Gamma}$ point, which corresponds to the λ_{SO} of Ru (see orange arrow near the $\bar{\Gamma}$ point in Figure 2b and 2f).

On the other hand, for the **M**⊥**z** state (the magnetization along the x axis or 100 direction), the spin states of the Ru d_{xz} and d_{yz} QWSs can be expressed by the up and down direction of the spin z component (that is, $|\uparrow - \downarrow\rangle/2$). Therefore, the leading order perturbation of $H_{SO}^{(z)}$ for the d_{xz} and d_{yz} QWSs becomes zero since $\langle\uparrow - \downarrow | \sigma_z | \uparrow - \downarrow\rangle = 0$. Consequently, the induced energy gap reduces to merely a few meV (see circles in Figure 2c and 2g). This band gap variation due to the different magnetization directions of **M**∥**z** and **M**⊥**z** results in a significant change in the density of state (DOS) as shown in Figure 2d and 2h. In Figure 2d, for instance, the **M**∥**z** state has a relatively smaller DOS at the Fermi level due to the SOC-induced energy gap in the QWS bands.

We note that the band structures and system energies of **M**∥**100** and **M**∥**110** are approximately the same as shown in Supporting Information Figure S5. This is due to the fact that both systems keep a vertical mirror symmetry. Therefore, we focus on the **M**∥**100** orientation, which in general represents the **M**⊥**z** behavior.

MAGNETOCRYSTALLINE ANISOTROPIC ENERGY AND QUANTUM WELL STATES

The dramatic differences in the DOS between the parallel and the perpendicular magnetization states (Figure 2d and 2h) have profound influences on the magnetocrystalline anisotropic energy. The MCAE is the energy discrepancy between these two magnetic states

https://doi.org/10.1021/acsanm.1c00775
ACS Appl. Nano Mater. 2021, 4, 5932−5939

$$\mathrm{MCAE} \equiv E_x - E_z \quad (2)$$

where E_x (E_z) is the total energy of the SRO ultrathin film with the magnetization **M**⊥**z** (**M**∥**z**). Our DFT calculations yield MCAE = 3. 73 and −2.01 meV for 6-u.c. and 9-u.c. SRO ultrathin films, respectively. The positive (negative) MCAE indicates the out-of-plane (in-plane) magnetization direction of the 6-u.c. (9-u.c.) SRO ultrathin films. As a result of SOC, the SRO ultrathin film selects a magnetization direction that can decrease the DOS at the Fermi level to reduce the total energy (Figure 2d and 2h). Here, we note that the total magnetic anisotropy energy (MAE) contains both the magnetocrystalline anisotropy energy (MCAE) and the magnetic dipole anisotropy energy (MDAE), namely, MAE = MCAE + MDAE. The MDAE is a perturbation in the total energy due to the magnetic dipole−dipole interaction in the system with **M**⊥**z** and **M**∥**z**.[59,60] Since the MCAE of the SRO ultrathin film in our calculation is an order of magnitude smaller than the MCAE (see Supporting Information), we thus ignore the impact of the MDAE on the magnetic anisotropy of SRO ultrathin films.

To demonstrate the evolution of the MCAE and QWSs energies of SRO thin films as a function of the film thickness, Figure 3a illustrates the energy of the d_{xz}−d_{yz} states at the $\bar{\Gamma}$

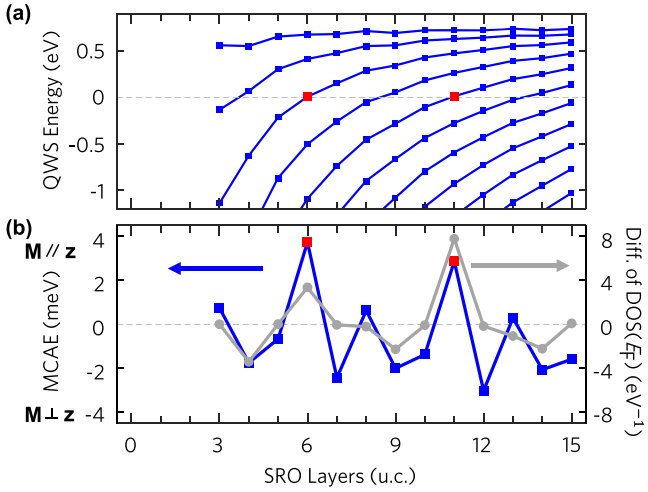

Figure 3. QWSs and MCAE of SRO ultrathin films. (a) Evolution of the QWS energies with different SRO thicknesses. Red dots indicate the QWS energies at the Fermi level. (b) MCAE (blue line) and DOS difference between two magnetization states (gray line). Positive MCAE indicates that the magnetization direction is perpendicular to the film. Red dots indicate the periodically appearing highest MCAE.

point to reflect the character of the t_{2g} band over the full Brillouin zone, similar to previous QWSs-related studies.[41,43,44,46,47] In this figure, the simulations start from three unit cells owing to the SRO ultrathin film present in nonmagnetic phase in one and two unit cells.[6] For the 3-u.c. SRO ultrathin film, only three QWSs with quantum numbers n = 1, 2, and 3 appear. As the film thickness increases, the QWS with the same quantum number shifts toward lower energy; therefore, the quantum number of the QWSs in the vicinity of the Fermi level increases. As shown in the red dots of Figure 3a, certain QWS thus is located almost at the Fermi level for special SRO thicknesses such as 6-u.c., 11-u.c., and so on. With the SOC included, these QWSs at the Fermi level split and generate the large positive MCAE in these SRO ultrathin films (thickness of 6-u.c. and 11-u.c.). Figure 3b illustrates the microscopic understanding of the MCAE origin by comparing the MCAE (blue squares) and the difference in DOS at the Fermi level between two magnetic states (gray dots). As can be seen, there exist correlations between the MCAE and the differences in DOS of the two magnetizations: The SOC introduces energy splittings in the QWSs at the Fermi level and yields significant differences in DOS, which finally results in the periodic MCAE oscillation with a large MCAE at specific SRO thicknesses. It has been observed in a 4 ML Fe that the magnetic anisotropy can be altered by 40% via applying a moderate gate voltage.[35] The screening effect in the Fe layer is stronger than that in an SRO layer since Fe is a better conductor. The amplitude of the MCAE oscillation in the SRO ultrathin film is four times larger than that in iron ultrathin films (Figure 3b), which is robust against thermal fluctuations. We can conclude that the SRO ultrathin film provides a better platform for controlling the magnetic anisotropy than the conventional ferromagnetic metal such as Fe.

MANIPULATING THE QWS AND MCAE BY APPLYING GATE VOLTAGE

Finally, we emphasize that the MCAE in SRO ultrathin films is not only geometrically tunable but also electronically controllable. To demonstrate such a capability of SRO ultrathin films, we vary the total electron number of a 6-u.c. SRO to simulate the doping effect as induced by an applied gate voltage in the MCAE and DOS difference between the two magnetization directions. As shown in Figure 4a, the undoped 6-u.c. SRO ultrathin film with positive MCAE between **M**⊥**z** and **M**∥**z** states of 3.73 meV prefers the out-of-plane magnetization direction. Under gate voltage-induced doping ranging from −0.04 to 0.12 e/Ru ion, the MCAE value decreases and finally switches the sign from positive to negative around 0.05 e/Ru, indicating the transition from out-of-plane to in-plane magnetization.

The DOS of the **M**⊥**z** and **M**∥**z** states with hole dopings of 0.017 and 0.083 e/Ru are shown in Figure 4b and 4c, respectively. For the hole doping case with 0.017 e/Ru as shown in Figure 4b, the situation is similar to the undoped case (Figure 2d): The SOC splits the QWS at the Fermi level, leading to a positive MCAE with the out-of-plane magnetization. When the hole doping increases to 0.083 e/Ru (Figure 4c), the Fermi level shifts moderately to a lower position, and thus, the DOS of **M**⊥**z** decreases to be smaller than that of **M**∥**z**. This eventually leads to the sign change in the MCAE and rotation of the easy axis from **M**∥**z** to **M**⊥**z**. The above-mentioned mechanism of how the QWS influences the MCAE is sketched in Figure 4d. Combinings Figure 3 and 4, our calculations clearly demonstrate that both the sign and the magnitude in the MCAE of a SRO ultrathin film can be controlled not only by the previously discussed film thickness but also by the electric modulation through applying a gate voltage or chemical doping. Similar behaviors are also expected in other oxide ultrathin films.

DISCUSSION

The origin of the large MCAE in Figure 3b is due to formation of the QWSs with d_{xz} and d_{yz} orbitals in SRO films. In the absence of SOC, these d_{xz} and d_{yz} SRO QWSs are degenerate at the $\bar{\Gamma}$ point due to the vertical mirror symmetry that has mirror planes perpendicular to the directions of (100), (010),

https://doi.org/10.1021/acsanm.1c00775
ACS Appl. Nano Mater. 2021, 4, 5932−5939

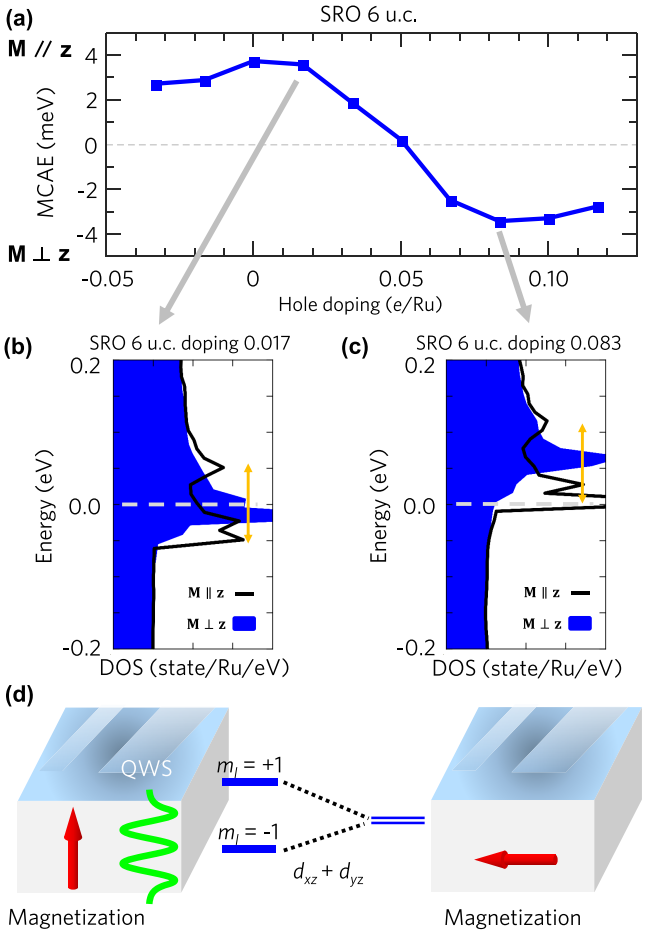

Figure 4. (a) MCAE of the 6-u.c. SRO film with doping ranging from −0.04 to 0.12 e/Ru ion. (b and c) DOS of **M**∥**z** (black curve) and **M**⊥**z** (blue area) states with hole doping of 0.017 and 0.083 e/Ru, respectively. (d) Sketch of the mechanism of how the QWS influences the MCAE. Easy axis of magnetization becomes **M**∥**z** (out-of-plane) when the energy of the QWS near the Fermi level with SOC splits the QWS energies. This MCAE can be tuned by changing the QWS energy by adjusting the film thickness and/or tuning the doping level by applying a gate voltage or chemical doping.

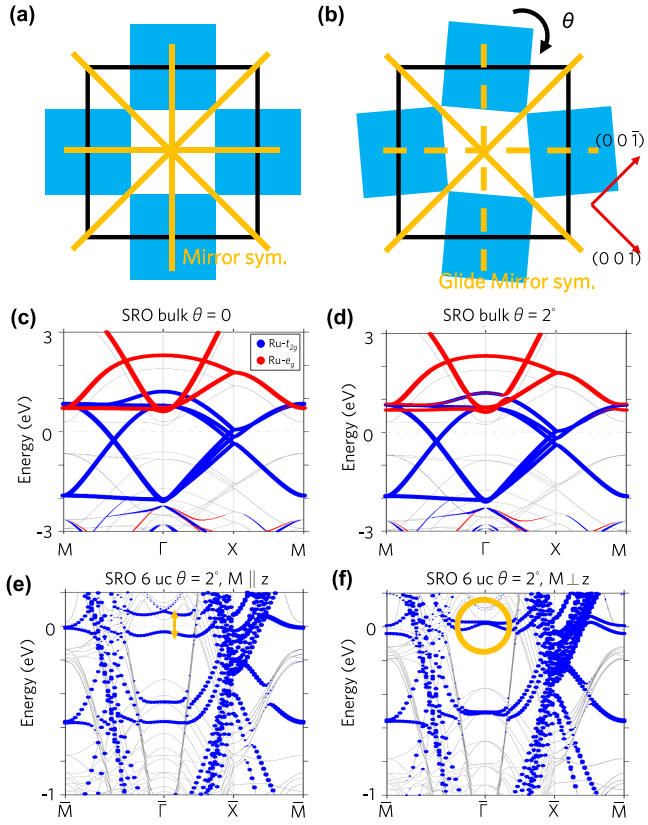

Figure 5. Top view of SRO with rotation angle (a) $\theta = 0$ and (b) $\theta = 2°$. Mirror symmetry is kept in both axes. (c) SRO bulk band structure with $\sqrt{2} \times \sqrt{2}$ lattice and rotation $\theta = 0$. (d) SRO bulk band with $\sqrt{2} \times \sqrt{2}$ lattice and rotation $\theta = 2°$. (e and f) Bands of SRO film with $\theta = 2°$ for **M**∥**z** and **M**⊥**z**, respectively.

$(\bar{1}00)$, and $(0\ \bar{1}0)$. When SOC is turned on and magnetization is perpendicular to the SRO film surface, all vertical mirror symmetry is broken, and hence, energy gaps between these QWSs are induced (see Figure 2).

We note that the rotation of RuO_6 octahedrons is neglected in our previous calculations from Figures 1−4 and may break vertical mirror symmetry, and this rotation appears in some SRO films.[18,61] To understand the impact of RuO_6 rotations in the lattice symmetry that crucially decides the MCAE, we separate the component of rotation in 3D as the in-plane angle θ and out-of-plane angle ϕ. Specifically, vertical mirror symmetry is kept when $\phi = 0$ and $\theta \neq 0$, see the solid lines in Figure 5b. For a SRO film on a $SrTiO_3$ (STO) substrate, for instance, it indeed has $\phi = 0$ because of a moderate in-plane strain due to STO substrate.[61] We calculate the bulk band structure of a distorted non-SOC SRO with $\phi = 0$ and $\theta = 2°$, and the Ru t_{2g} bands remain degenerate at the $\bar{\Gamma}$ point due to the vertical mirror symmetry being kept, as shown in Figure 5d.

We further calculate the 6-u.c. SRO film with SOC and rotation angles $\phi = 0$ and $\theta = 2°$. Its band structure with magnetization perpendicular and parallel to the film surface is illustrated in Figure 5e and 5f, respectively. The change of the QWSs band gaps between Figure 5e and Figure 5f is the same as that between Figure 2b and Figure 2c, and the position of the QWSs are approximately the same in this film with and without the RuO_6 rotation. As the result of the rotation of RuO_6 octahedrons in an SRO film, the nature of the MCAE is the same and the MCAE value changes moderately when the angle θ appears (see Figure S2 in Supporting Information). We also investigate the MCAE with respect to other realistic samples, including a SRO ultrathin film with compressed in-plane lattice structure due to different substrate (see Figure S3 in Supporting Information) and is placed on a the STO substrate (see Figure S4 in the Supporting Information). In these systems, the peaks in the MCAE oscillation change mildly and features of the MCAE remain the same as that in Figure 3b because the nature of the spin-polarized SRO QWSs is kept.

CONCLUSIONS

The correlations between the rich QWSs and the MCAE have been studied widely in different ferromagnetic materials such as iron and cobalt in pioneer works.[24,25,28,29] For the first time, we theoretically establish a clear direct relation between the MCAE and the spin-polarized QWSs (see Figure 3). The half-metallic nature of SRO provides an excellent platform for studying the relations among SOC, the QWS, and the MCAE. We show in this work that the MCAE oscillates with the SRO film thickness periodically due to the minority d_{xz} and d_{yz}

https://doi.org/10.1021/acsanm.1c00775
ACS Appl. Nano Mater. 2021, 4, 5932−5939

QWSs that are susceptible to intrinsic SOC. The amplitude of the MCAE oscillation in a SRO ultrathin film is an order larger than that in iron ultrathin films, which is robust against thermal fluctuations. Moreover, we demonstrate that both the sign and the magnitude of the MCAE can be tuned through controlling the QWSs not only geometrically by adjusting the film thickness but also electrically by tuning the doping level via applying a gate voltage or chemical doping. These important findings show that the easy axis of SRO thin film is structurally, electrically, and/or chemically tunable.

Our results explain the key features of the MCAE observed in SRO films in the experimental studies, including a large MCAE and a switchable easy axis crucially depend on detailed system conditions. In previous experiments, the MCAE of a $SrRuO_3$ ultrathin film with a thickness of over 700 Å, or over 175 layers, has been reported.[62,63] Our study encourages scientists to measure the MCAE in ultrathin SRO films. We confirmed that the same exotic MCAE nature appears in a general SRO film that has rotation of RuO_6 octahedrons with a changed in-plane lattice constant or on a substrate. The important findings in this work on the SRO/ferroelectric heterostructure[9,10] show that electric properties are fine tuned by varying the gate voltage and can be related to the spin-polarized QWSs when the strain effect is moderate.

Finally, we propose the proper experimental systems for examining our predictions on the tunable large magnetic anisotropy in SRO ultrathin films. Our model SRO ultrathin films have two key features: a tetragonal lattice structure and a small Ru−O−Ru angle that is equal to or smaller than 2°. The tetragonal SRO thin film with a lattice constant that is the same as in our calculation (3.93 Å) has been manufactured.[23] Besides, the Ru−O−Ru angle is very small and can be approximately neglected for the SRO ultrathin film on a STO substrate.[64] These SRO films provide suitable playgrounds to fulfill the tunability of the large magnetic anisotropy. This prediction in our simulations have—in view of the large magnetic anisotropy in the SRO ultrathin film—shows great promise in achieving a spintronic device such as storage and memory devices with size on the nanoscale.

METHOD

First-principles calculations were performed using the Vienna Ab-initio Simulation Package (VASP)[65] based on density functional theory (DFT). The projector augmented wave (PAW)[66,67] pseudopotential was adopted in the local spin density approximation (LSDA) with the Ceperley−Alder[68] and Perdew−Zunger[69] (CA−PZ) exchange-correlation functional. The on-site Coulomb repulsion U = 3.5 eV and exchange parameter J = 0.6 eV for Ru d states[54] were used in the rotationally invariant LDA+U scheme.[70] The k mesh of 24 × 24 × 1 over the two-dimensional Brillouin zone with a cutoff energy of 400 eV for the plane waves was used. Spin−orbital coupling (SOC) was included in the calculations. The energy convergence upon the density of the k mesh and cutoff energy was carefully checked for the MCAE calculations of SRO ultrathin films.

ASSOCIATED CONTENT

Supporting Information

The Supporting Information is available free of charge at https://pubs.acs.org/doi/10.1021/acsanm.1c00775.

Magnetic dipole anisotropy energy and average of the magnetic moment of SRO ultrathin film; MAE with rotation of RuO_6 octahedron; MAE of SRO with the different lattice constant; band structure of SRO ultrathin film with **M**||(110) (PDF)

AUTHOR INFORMATION

Corresponding Authors

Horng-Tay Jeng − *Department of Physics, National Tsing Hua University, Hsinchu 30013, Taiwan; Physics Division, National Center for Theoretical Sciences, Hsinchu 30013, Taiwan; Institute of Physics, Academia Sinica, Taipei 11529, Taiwan;* orcid.org/0000-0002-2881-3826; Email: jeng@phys.nthu.edu.tw

Ching-Hao Chang − *Department of Physics, National Cheng Kung University, Tainan 70101, Taiwan; Center for Quantum Frontiers of Research & Technology (QFort), National Cheng Kung University, Tainan 70101, Taiwan;* orcid.org/0000-0003-0878-9328; Email: cutygo@phys.ncku.edu.tw

Author

Angus Huang − *Department of Physics, National Tsing Hua University, Hsinchu 30013, Taiwan*

Complete contact information is available at: https://pubs.acs.org/10.1021/acsanm.1c00775

Notes

The authors declare no competing financial interest.

ACKNOWLEDGMENTS

This work was supported by the Ministry of Science and Technology, Taiwan (Grant nos. MOST 106-2112-M-007-012-MY3, 107-2112-M-006-025-MY3, 108-2638-M-006-002-MY2, and 109-2112-M-007-034-MY3). J.H.T. is also thankful for support from NCHC, CINC-NTU, AS-iMATE-109-13, and CQT-NTHU-MOE, Taiwan. C.H.C. acknowledges support by the Yushan Young Scholar Program under the Ministry of Education (MOE) in Taiwan.

REFERENCES

(1) Kent, A. D.; Worledge, D. C. A new spin on magnetic memories. *Nat. Nanotechnol.* **2015**, *10*, 187.

(2) Slonczewski, J. C. Conductance and exchange coupling of two ferromagnets separated by a tunneling barrier. *Phys. Rev. B: Condens. Matter Mater. Phys.* **1989**, *39*, 6995−7002.

(3) Fang, D.; Kurebayashi, H.; Wunderlich, J.; Výborný, K.; Zârbo, L. P.; Campion, R. P.; Casiraghi, A.; Gallagher, B. L.; Jungwirth, T.; Ferguson, A. J. Spin-orbit-driven ferromagnetic resonance. *Nat. Nanotechnol.* **2011**, *6*, 413.

(4) Sankey, J. C.; Cui, Y.-T.; Sun, J. Z.; Slonczewski, J. C.; Buhrman, R. A.; Ralph, D. C. Measurement of the spin-transfer-torque vector in magnetic tunnel junctions. *Nat. Phys.* **2008**, *4*, 67.

(5) Si, L.; Janson, O.; Li, G.; Zhong, Z.; Liao, Z.; Koster, G.; Held, K. Quantum anomalous hall state in ferromagnetic $SrRuO_3$ (111) bilayers. *Phys. Rev. Lett.* **2017**, *119*, 026402.

(6) Chang, Y. J.; Kim, C. H.; Phark, S.-H.; Kim, Y. S.; Yu, J.; Noh, T. W. Fundamental thickness limit of itinerant ferromagnetic $SrRuO_3$ thin films. *Phys. Rev. Lett.* **2009**, *103*, 057201.

(7) Brataas, A.; Kent, A. D.; Ohno, H. Current-induced torques in magnetic materials. *Nat. Mater.* **2012**, *11*, 372.

(8) Soumyanarayanan, A.; Reyren, N.; Fert, A.; Panagopoulos, C. Emergent phenomena induced by spin-orbit coupling at surfaces and interfaces. *Nature* **2016**, *539*, 509.

(9) Zheng, W.; Wang, Y.; Jin, C.; Yin, R.; Li, D.; Wang, P.; Liu, S.; Wang, X.; Zheng, D.; Bai, H. Ferroelectric resistance switching in Pt/Fe/BiFeO3/SrRuO3/SrTiO3 heterostructures. *Phys. Chem. Chem. Phys.* **2020**, *22*, 13277−13284.
(10) Ren, Z.; Shao, F.; Liu, P.; Wang, M.; Chen, J.; Meng, K.; Xu, X.; Miao, J.; Jiang, Y. Nonvolatile ferroelectric field control of the anomalous hall effect in bifeo$_3$/srruo$_3$ bilayer. *Phys. Rev. Appl.* **2020**, *13*, 024044.
(11) Zheng, M.; Li, X.; Xiao, W.; Wang, W.; Ni, H. Oxygen deficiency and cooling field driven vertical hysteretic shift in epitaxial SrRuO3/SrTiO3 heterostructures. *Appl. Phys. Lett.* **2017**, *111*, 152405.
(12) Zheng, M.; Wang, W. Tunable Ferromagnetic Transition Temperature and Vertical Hysteretic Shift in SrRuO3 Films Integrated on Si(001). *ACS Appl. Mater. Interfaces* **2016**, *8* (22), 14012−14018.
(13) Kanbayasi, A. Magnetic properties of new cubic-perovskite mixtures; $(La_{0.5}Na_{0.5})RuO_3$ and $(Ca_{1-x}A_x)RuO_3$ (A = Mg, Sr). *J. Phys. Soc. Jpn.* **1978**, *44* (1), 108−113.
(14) Kanbayasi, A. Magnetocrystalline anisotropy of $SrRuO_3$. *J. Phys. Soc. Jpn.* **1976**, *41* (6), 1879−1883.
(15) Kats, Y.; Genish, I.; Klein, L.; Reiner, J. W.; Beasley, M. R. Large anisotropy in the paramagnetic susceptibility of $SrRuO_3$ films. *Phys. Rev. B: Condens. Matter Mater. Phys.* **2005**, *71*, 100403.
(16) Gan, Q.; Rao, R. A.; Eom, C. B.; Wu, L.; Tsui, F. Lattice distortion and uniaxial magnetic anisotropy in single domain epitaxial (110) films of $SrRuO_3$. *J. Appl. Phys.* **1999**, *85* (8), 5297−5299.
(17) Herranz, G.; Sánchez, F.; Dix, N.; Hrabovsky, D.; Infante, I. C.; Fontcuberta, J.; García-Cuenca, M. V.; Ferrater, C.; Varela, M. Controlled magnetic anisotropy of $SrRuO_3$ thin films grown on nominally exact $SrTiO_3$(001) substrates. *Appl. Phys. Lett.* **2006**, *89* (15), 152501.
(18) Koster, G.; Klein, L.; Siemons, W.; Rijnders, G.; Dodge, J. S.; Eom, C.-B.; Blank, D. H. A.; Beasley, M. R. Structure, physical properties, and applications of $SrRuO_3$ thin films. *Rev. Mod. Phys.* **2012**, *84*, 253−298.
(19) Snyder, G. J. Critical behavior and anisotropy in single crystal $SrRuO_3$. *ArXiv* **2019**, *1904*, 12193.
(20) Kan, D.; Wakabayashi, Y.; Tajiri, H.; Shimakawa, Y. Interfacially engineered oxygen octahedral rotations and their impact on strain relief in coherently grown $SrRuO_3$ films. *Phys. Rev. B: Condens. Matter Mater. Phys.* **2016**, *94*, 024112.
(21) Kan, D.; Mizumaki, M.; Nishimura, T.; Shimakawa, Y. Orbital magnetic moments in $SrRuO_3$ epitaxial thin films with interfacially controlled magnetic anisotropy. *Phys. Rev. B: Condens. Matter Mater. Phys.* **2016**, *94*, 214420.
(22) Ishigami, K.; Yoshimatsu, K.; Toyota, D.; Takizawa, M.; Yoshida, T.; Shibata, G.; Harano, T.; Takahashi, Y.; Kadono, T.; Verma, V. K.; Singh, V. R.; Takeda, Y.; Okane, T.; Saitoh, Y.; Yamagami, H.; Koide, T.; Oshima, M.; Kumigashira, H.; Fujimori, A. Thickness-dependent magnetic properties and strain-induced orbital magnetic moment in $SrRuO_3$ thin films. *Phys. Rev. B: Condens. Matter Mater. Phys.* **2015**, *92*, 064402.
(23) Herklotz, A.; Kataja, M.; Nenkov, K.; Biegalski, M. D.; Christen, H.-M.; Deneke, C.; Schultz, L.; Dörr, K. Magnetism of the tensile-strain-induced tetragonal state of $SrRuO_3$ films. *Phys. Rev. B: Condens. Matter Mater. Phys.* **2013**, *88*, 144412.
(24) Przybylski, M.; Dabrowski, M.; Bauer, U.; Cinal, M.; Kirschner, J. Oscillatory magnetic anisotropy due to quantum well states in thin ferromagnetic films (invited). *J. Appl. Phys.* **2012**, *111* (7), 07C102.
(25) Guo, G. Y. Magnetocrystalline anisotropy oscillations predicted in Fe/Au(001) superlattices. *J. Phys.: Condens. Matter* **1999**, *11*, 4329−4334.
(26) Sandratskii, L. M. Correlated oscillations of the magnetic anisotropy energy and orbital moment anisotropy in thin films: The role of quantum well states. *Phys. Rev. B: Condens. Matter Mater. Phys.* **2015**, *92*, 134414.
(27) Atodiresei, N.; Dederichs, P. H.; Mokrousov, Y.; Bergqvist, L.; Bihlmayer, G.; Blügel, S. Controlling the magnetization direction in molecules via their oxidation state. *Phys. Rev. Lett.* **2008**, *100*, 117207.
(28) Weber, W.; Bischof, A.; Allenspach, R.; Würsch, C.; Back, C. H.; Pescia, D. Oscillatory magnetic anisotropy and quantum well states in Cu/Co/Cu(100) films. *Phys. Rev. Lett.* **1996**, *76*, 3424−3427.
(29) Bauer, U.; Przybylski, M.; Beach, G. S. D. Voltage control of magnetic anisotropy in fe films with quantum well states. *Phys. Rev. B: Condens. Matter Mater. Phys.* **2014**, *89*, 174402.
(30) Młyńczak, E.; Eschbach, M.; Borek, S.; Minár, J.; Braun, J.; Aguilera, I.; Bihlmayer, G.; Döring, S.; Gehlmann, M.; Gospodarič, P.; Suga, S.; Plucinski, L.; Blügel, S.; Ebert, H.; Schneider, C. M. Fermi surface manipulation by external magnetic field demonstrated for a prototypical ferromagnet. *Phys. Rev. X* **2016**, *6*, 041048.
(31) Chantis, A. N.; Belashchenko, K. D.; Tsymbal, E. Y.; van Schilfgaarde, M. Tunneling anisotropic magnetoresistance driven by resonant surface states: First-principles calculations on an Fe(001) surface. *Phys. Rev. Lett.* **2007**, *98*, 046601.
(32) Gambardella, P.; Stepanow, S.; Dmitriev, A.; Honolka, J.; de Groot, F. M. F.; Lingenfelder, M.; Gupta, S. S.; Sarma, D. D.; Bencok, P.; Stanescu, S.; Clair, S.; Pons, S.; Lin, N.; Seitsonen, A. P.; Brune, H.; Barth, J. V.; Kern, K. Supramolecular control of the magnetic anisotropy in two-dimensional high-spin fe arrays at a metal interface. *Nat. Mater.* **2009**, *8*, 189.
(33) Yang, H. X.; Chshiev, M.; Dieny, B.; Lee, J. H.; Manchon, A.; Shin, K. H. First-principles investigation of the very large perpendicular magnetic anisotropy at felmgo and colmgo interfaces. *Phys. Rev. B: Condens. Matter Mater. Phys.* **2011**, *84*, 054401.
(34) Mihai Miron, I.; Gaudin, G.; Auffret, S.; Rodmacq, B.; Schuhl, A.; Pizzini, S.; Vogel, J.; Gambardella, P. Current-driven spin torque induced by the rashba effect in a ferromagnetic metal layer. *Nat. Mater.* **2010**, *9*, 230.
(35) Maruyama, T.; Shiota, Y.; Nozaki, T.; Ohta, K.; Toda, N.; Mizuguchi, M.; Tulapurkar, A. A.; Shinjo, T.; Shiraishi, M.; Mizukami, S.; Ando, Y.; Suzuki, Y. Large voltage-induced magnetic anisotropy change in a few atomic layers of iron. *Nat. Nanotechnol.* **2009**, *4*, 158.
(36) Ikeda, S.; Miura, K.; Yamamoto, H.; Mizunuma, K.; Gan, H. D.; Endo, M.; Kanai, S.; Hayakawa, J.; Matsukura, F.; Ohno, H. A perpendicular-anisotropy cofeb-mgo magnetic tunnel junction. *Nat. Mater.* **2010**, *9*, 721.
(37) Chang, C.-H.; Dou, K.-P.; Guo, G.-Y.; Kaun, C.-C. Quantum-well-induced engineering of magnetocrystalline anisotropy in ferromagnetic films. *NPG Asia Mater.* **2017**, *9*, e424.
(38) Cinal, M.; Edwards, D. M.; Mathon, J. Magnetocrystalline anisotropy in ferromagnetic films. *Phys. Rev. B: Condens. Matter Mater. Phys.* **1994**, *50*, 3754−3760.
(39) Kang, S.; Tseng, Y.; Kim, B. H.; Yun, S.; Sohn, B.; Kim, B.; McNally, D.; Paris, E.; Kim, C. H.; Kim, C.; Noh, T. W.; Ishihara, S.; Schmitt, T.; Park, J.-G. Orbital-selective confinement effect of ru 4d orbitals in $SrRuO_3$ ultrathin film. *Phys. Rev. B: Condens. Matter Mater. Phys.* **2019**, *99*, 045113.
(40) Luh, D.-A.; Miller, T.; Paggel, J. J.; Chou, M. Y.; Chiang, T.-C. Quantum electronic stability of atomically uniform films. *Science* **2001**, *292* (5519), 1131−1133.
(41) Tang, S.-J.; Chang, W.-K.; Chiu, Y.-M.; Chen, H.-Y.; Cheng, C.-M.; Tsuei, K.-D.; Miller, T.; Chiang, T.-C. Enhancement of subband effective mass in Ag/Ge(111) thin film quantum wells. *Phys. Rev. B: Condens. Matter Mater. Phys.* **2008**, *78*, 245407.
(42) Tang, S.-J.; Lee, C.-Y.; Huang, C.-C.; Chang, T.-R.; Cheng, C.-M.; Tsuei, K.-D.; Jeng, H.-T. Bilayer oscillation of subband effective masses in Pb/Ge(111) thin-film quantum wells. *Appl. Phys. Lett.* **2010**, *96* (10), 103106.
(43) Paggel, J. J.; Wei, C. M.; Chou, M. Y.; Luh, D.-A.; Miller, T.; Chiang, T.-C. Atomic-layer-resolved quantum oscillations in the work function: Theory and experiment for Ag/Fe(100). *Phys. Rev. B: Condens. Matter Mater. Phys.* **2002**, *66*, 233403.
(44) Liu, R.-Y.; Huang, A.; Huang, C.-C.; Lee, C.-Y.; Lin, C.-H.; Cheng, C.-M.; Tsuei, K.-D.; Jeng, H.-T.; Matsuda, I.; Tang, S.-J.

https://doi.org/10.1021/acsanm.1c00775
ACS Appl. Nano Mater. 2021, 4, 5932−5939

Deeper insight into phase relations in ultrathin Pb films. *Phys. Rev. B: Condens. Matter Mater. Phys.* **2015**, *92*, 115415.
(45) Czoschke, P.; Hong, H.; Basile, L.; Chiang, T.-C. Quantum beating patterns observed in the energetics of Pb film nanostructures. *Phys. Rev. Lett.* **2004**, *93*, 036103.
(46) Wei, C. M.; Chou, M. Y. Theory of quantum size effects in thin Pb(111) films. *Phys. Rev. B: Condens. Matter Mater. Phys.* **2002**, *66*, 233408.
(47) Chang, C.-H.; Dou, K.-P.; Chen, Y.-C.; Hong, T.-M.; Kaun, C.-C. Engineering the interlayer exchange coupling in magnetic trilayers. *Sci. Rep.* **2015**, *5*, 16844.
(48) Guo, Y.; Zhang, Y.-F.; Bao, X.-Y.; Han, T.-Z.; Tang, Z.; Zhang, L.-X.; Zhu, W.-G.; Wang, E. G.; Niu, Q.; Qiu, Z. Q.; et al. Superconductivity modulated by quantum size effects. *Science* **2004**, *306* (5703), 1915−1917.
(49) Qin, S.; Kim, J.; Niu, Q.; Shih, C.-K. Superconductivity at the two-dimensional limit. *Science* **2009**, *324* (5932), 1314−1317.
(50) Lu, W.; Yang, P.; Song, W. D.; Chow, G. M.; Chen, J. S. Control of oxygen octahedral rotations and physical properties in $SrRuO_3$ films. *Phys. Rev. B: Condens. Matter Mater. Phys.* **2013**, *88*, 214115.
(51) Kan, D.; Aso, R.; Sato, R.; Haruta, M.; Kurata, H.; Shimakawa, Y. Tuning magnetic anisotropy by interfacially engineering the oxygen coordination environment in a transition metal oxide. *Nat. Mater.* **2016**, *15*, 432.
(52) Chang, S. H.; Chang, Y. J.; Jang, S. Y.; Jeong, D. W.; Jung, C. U.; Kim, Y.-J.; Chung, J.-S.; Noh, T. W. Thickness-dependent structural phase transition of strained $SrRuO_3$ ultrathin films: The role of octahedral tilt. *Phys. Rev. B: Condens. Matter Mater. Phys.* **2011**, *84*, 104101.
(53) Wang, L.; Feng, Q.; Kim, Y.; Kim, R.; Lee, K. H.; Pollard, S. D.; Shin, Y. J.; Zhou, H.; Peng, W.; Lee, D. Ferroelectrically tunable magnetic skyrmions in ultrathin oxide heterostructures. *Nat. Mater.* **2018**, *17* (12), 1087−1094.
(54) Jeng, H.-T.; Lin, S.-H.; Hsue, C.-S. Orbital ordering and jahn-teller distortion in perovskite ruthenate $SrRuO_3$. *Phys. Rev. Lett.* **2006**, *97*, 067002.
(55) Ryee, S.; Jang, S. W.; Kino, H.; Kotani, T.; Han, M. J. Quasiparticle self-consistent gw calculation of Sr_2RuO_4 and $SrRuO_3$. *Phys. Rev. B: Condens. Matter Mater. Phys.* **2016**, *93*, 075125.
(56) Raychaudhuri, P.; Mackenzie, A. P.; Reiner, J. W.; Beasley, M. R. Transport spin polarization in $SrRuO_3$ measured through point-contact andreev reflection. *Phys. Rev. B: Condens. Matter Mater. Phys.* **2003**, *67*, 020411.
(57) Sanders, J.; Woods, G. T.; Poddar, P.; Srikanth, H.; Dabrowski, B.; Kolesnik, S. Spin polarization measurements on polycrystalline strontium ruthenates using point-contact andreev reflection. *J. Appl. Phys.* **2005**, *97* (10), 10C912.
(58) Nadgorny, B.; Osofsky, M. S.; Singh, D. J.; Woods, G. T.; Soulen, R. J.; Lee, M. K.; Bu, S. D.; Eom, C. B. Measurements of spin polarization of epitaxial $SrRuO_3$ thin films. *Appl. Phys. Lett.* **2003**, *82* (3), 427.
(59) Guo, G. Y.; Temmerman, W. M.; Ebert, H. First-principles determination of the magnetization direction of fe monolayer in noble metals. *J. Phys.: Condens. Matter* **1991**, 3 (42), 8205.
(60) Tung, J. C.; Guo, G. Y. Magnetic moment and magnetic anisotropy of linear and zigzag 4d and 5d transition metal nanowires: First-principles calculations. *Phys. Rev. B: Condens. Matter Mater. Phys.* **2010**, *81*, 094422.
(61) Gu, M.; Xie, Q.; Shen, X.; Xie, R.; Wang, J.; Tang, G.; Wu, D.; Zhang, G. P.; Wu, X. S. Magnetic ordering and structural phase transitions in a strained ultrathin $SrRuO_3/SrTiO_3$ superlattice. *Phys. Rev. Lett.* **2012**, *109*, 157003.
(62) Wang, X. W.; Wang, X.; Zhang, Y. Q.; Zhu, Y. L.; Wang, Z. J.; Zhang, Z. D. Magnetic anisotropy and metal-insulator transition in $SrRuO_3$ thin films at different growth temperatures. *J. Appl. Phys.* **2010**, *107* (11), 113925.
(63) Wang, X. W.; Zhang, Y. Q.; Meng, H.; Wang, Z. J.; Li, D.; Zhang, Z. D. Magnetic anisotropy and transport properties of 70 nm $SrRuO_3$ films grown on different substrates. *J. Appl. Phys.* **2011**, *109* (7), 07D707.
(64) Lin, S.; Zhang, Q.; Roldan, M. A.; Das, S.; Charlton, T.; Fitzsimmons, M. R.; Jin, Q.; Li, S.; Wu, Z.; Chen, S.; Guo, H.; Tong, X.; He, M.; Ge, C.; Wang, C.; Gu, L.; Jin, K.-j.; Guo, E.-J. Switching magnetic anisotropy of $SrRuO_3$ by capping-layer-induced octahedral distortion. *Phys. Rev. Appl.* **2020**, *13*, 034033.
(65) Kresse, G.; Furthmüller, J. Efficiency of ab-initio total energy calculations for metals and semiconductors using a plane-wave basis set. *Comput. Mater. Sci.* **1996**, *6* (1), 15.
(66) Kresse, G.; Joubert, D. From ultrasoft pseudopotentials to the projector augmented-wave method. *Phys. Rev. B: Condens. Matter Mater. Phys.* **1999**, *59*, 1758.
(67) Blöchl, P. E. Projector augmented-wave method. *Phys. Rev. B: Condens. Matter Mater. Phys.* **1994**, *50*, 17953.
(68) Ceperley, D. M.; Alder, B. J. Ground state of the electron gas by a stochastic method. *Phys. Rev. Lett.* **1980**, *45*, 566.
(69) Perdew, J. P.; Zunger, A. Self-interaction correction to density-functional approximations for many-electron systems. *Phys. Rev. B: Condens. Matter Mater. Phys.* **1981**, *23*, 5048−5079.
(70) Liechtenstein, A. I.; Anisimov, V. I.; Zaanen, J. Density-functional theory and strong interactions: Orbital ordering in mott-hubbard insulators. *Phys. Rev. B: Condens. Matter Mater. Phys.* **1995**, *52*, R5467.

https://doi.org/10.1021/acsanm.1c00775
ACS Appl. Nano Mater. 2021, 4, 5932−5939